ADVANCED FUNCTIONAL MATERIALS
www.afm-journal.de

ADVANCED SCIENCE NEWS
www.advancedsciencenews.com

Stretchable Capacitive Sensors of Torsion, Strain, and Touch Using Double Helix Liquid Metal Fibers

*Christopher B. Cooper, Kuralamudhan Arutselvan, Ying Liu, Daniel Armstrong, Yiliang Lin, Mohammad Rashed Khan, Jan Genzer, and Michael D. Dickey**

Soft and stretchable sensors have the potential to be incorporated into soft robotics and conformal electronics. Liquid metals represent a promising class of materials for creating these sensors because they can undergo large deformations while retaining electrical continuity. Incorporating liquid metal into hollow elastomeric capillaries results in fibers that can integrate with textiles, comply with complex surfaces, and be mass produced at high speeds. Liquid metal is injected into the core of hollow and extremely stretchable elastomeric fibers and the resulting fibers are intertwined into a helix to fabricate capacitive sensors of torsion, strain, and touch. Twisting or elongating the fibers changes the geometry and, thus, the capacitance between the fibers in a predictable way. These sensors offer a simple mechanism to measure torsion up to 800 rad m^{-1}—two orders of magnitude higher than current torsion sensors. These intertwined fibers can also sense strain capacitively. In a complementary embodiment, the fibers are injected with different lengths of liquid metal to create sensors capable of distinguishing touch along the length of a small bundle of fibers via self-capacitance. The three capacitive-based modes of sensing described here may enable new sensing applications that employ the unique attributes of stretchable fibers.

1. Introduction

This paper describes the use of stretchable hollow elastomeric fibers filled with liquid metal (LM) as soft and stretchable capacitive sensors of torsion, strain, and touch. Sensors that are soft and stretchable are useful for soft robotics as well as wearable, conformable, and deformable electronic devices. Although most commercial sensors are built from rigid materials, there are a number of emerging strategies for creating stretchable devices capable of sensing various biometrics[1–6] as well as mechanical deformations such as tensile strain,[2,7,8] bending,[2,4,9] and torsion.[2,9]

LMs, such as eutectic gallium indium (EGaIn, 75% Ga and 25% In), offer a promising way to create such sensors.[10] EGaIn has low toxicity,[11] negligible vapor pressure at room temperature, and low viscosity. The latter property allows LM to flow in response to deformation, whereas solid metals are stiff and prone to fail at small strains. Embedding LM in elastomer decouples the electrical and mechanical properties; that is, these composites have the electrical properties of the metal and the mechanical properties of the elastomer. Incorporating the LM into the hollow core of an elastomeric fiber results in a useful form for sensors because fibers may be integrated into clothing and fabrics.[12–15] Furthermore, fibers are inherently flexible, compliant, and conformal due to their narrow cross-section. Thus, fibers can readily wrap onto and conform to surfaces with Gaussian curvature whereas 2D sheets cannot without significant deformation. Fibers can also be mass produced at high speeds with small diameters (hundreds of microns) and produced by hand in a laboratory environment at room temperature.[16] The fibers described in this work have the additional advantage of being built from stretchable and soft materials. Fibers with LM cores have previously been used to make light-emitting structures[17] and stretchable wires that retain metallic conductance up to ≈800% strain.[18] We reasoned that elastomeric fibers filled with LM could also be used for capacitive sensing of torsion, strain, and touch.

Here, we intertwined two fibers into a double-helix to create sensors of both torsion and strain since twisting or stretching the fibers increases the contact area between them, and therefore changes the capacitance. The complexity of torsion, which causes both normal and shear strain, has previously precluded the development of a simple sensor capable of measuring a large range of torsion. Existing torsion sensors measure changes in normalized resistance,[2,8,19,20] pressure,[9] and optical properties,[21] or utilize surface acoustic waves[22] or the inverse magnetostrictive effect.[23] Some of these sensors can detect changes as small as 0.3 rad m^{-1} and can measure torsion up to 800 rad m^{-1} before failure. Most existing torsion sensors, however, are rigid, cumbersome, expensive, and complex. The soft and stretchable sensor developed here offers a simple mechanism to measure large changes in torsion which may be useful for unconventional robotics[24,25] or artificial muscles.[26]

In addition to sensing torsion, intertwined fibers increase capacitance in response to strain due to the increase in contact

C. B. Cooper, K. Arutselvan, Dr. Y. Liu, D. Armstrong, Y. Lin, Dr. M. R. Khan, Prof. J. Genzer, Prof. M. D. Dickey
Department of Chemical & Biomolecular Engineering
North Carolina State University
Raleigh, NC 27695-7905, USA
E-mail: mddickey@ncsu.edu

DOI: 10.1002/adfm.201605630

area from elongation. There is growing interest in stretchable sensors capable of measuring large strains (above 30%) relative to conventional strain sensors.[27–33] Most existing stretchable strain sensors measure resistance[8,34–41] or capacitance;[42–49] the latter occurs due to mechanical deformations that decrease the distance between electrodes or increase the electrode area. Capacitive strain sensors have gauge factors (from 0.004 to 1) that do not vary over large ranges of strains (from 35% to 300%),[42–48] and thus offer a promising mechanism to create stretchable strain sensors.

Intertwined fibers with LM cores also offer the opportunity to sense touch using self-capacitance. Capacitance is a commonly used measurement for many touch sensors including commercial touch screens, and previously it has been utilized to create soft touch sensors.[45,50–55] Such sensors have geometries of pads or woven fiber grids, but a capacitive touch sensor that can differentiate touch along its length is yet to be implemented in a strictly fiber shape or using ultrastretchable materials.

Here, we describe capacitive sensors of torsion, touch, and strain composed of intertwined core–shell LM, elastomeric polymer fibers. This approach is noteworthy due to (1) the ability of the sensor to detect changes in torsion up to 10 800 rad m^{-1} (i.e., two orders of magnitude higher than current torsion sensors); (2) the simplicity of the capacitive sensing mechanism for measuring torsion, strain, and touch; (3) the fabrication of a fiber capable of differentiating touch along its length; (4) the versatility of the fiber form factor; and (5) the soft and stretchable mechanical properties of the sensor. This paper discusses the capabilities and limitations of these capacitive fiber sensors along with a geometric model to predict changes in capacitance as a function of torsion and strain.

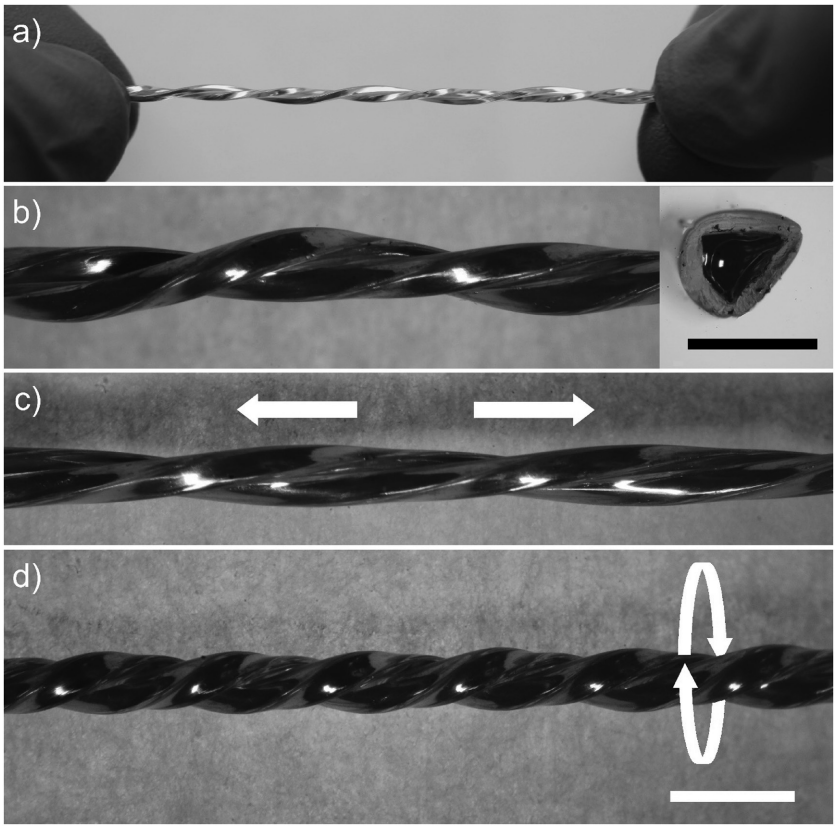

Figure 1. Photographs of two twisted fibers with 850 µm diameter. a) Photograph of twisted fibers held in fingers. b) A pair of intertwined fibers with a torsional level of 630 rad m^{-1}. LM fills the core of the fiber cross-section (inset; scale bar: 1 mm). c) Stretching the fibers to 150% strain reduces the torsional level to 420 rad m^{-1}. d) Additional twisting increases the torsional level to 1260 rad m^{-1}. The scale bar for (b–d) is 2.5 mm.

2. Results and Discussion

Figure 1a shows a pair of fibers intertwined in a double helix and Figure 1b shows a closer image of the two fibers (850 µm diameter) twisted to 630 rad m^{-1}, along with an inset image of the fiber cross-section. Figure 1c,d shows images of these fibers being stretched to 150% strain or twisted to 1260 rad m^{-1}, respectively. To fabricate the hollow fibers, we melt-extruded Hytrel (DuPont TPC Hytrel 6356 63 Shore) through a die, into a water bath for cooling, and onto a collection roll using a process similar to our previous report.[18] The fibers pictured in Figure 1 have triangular cross-sections with wall thickness of ≈160 µm and side length of ≈850 µm. We also used fibers with wall thicknesses of ≈70 and ≈55 µm and side lengths of ≈350 and ≈235 µm, respectively. Although we did not intentionally seek this geometry (it is a result of the shape of the die), triangular cross-sections have been shown previously to minimize nonlinearity and hysteresis in pressure sensing using elastomeric channels filled with LM.[56] We injected EGaIn into the fibers with a needle-tipped syringe. Inserting copper wire into the ends of the fiber created electrical connections sealed with adhesive (Norland NOA 61).

2.1. Torsion Sensor

Figure 2a illustrates the basic concept of the torsion sensor; twisting two EGaIn-filled fibers, while keeping the end-to-end distance (L) constant, changes the geometry between the fibers and therefore changes the capacitance. As we show here, the dominant change to the geometry is the increased distance traversed by the fiber (ζ) for a given end-to-end distance. To quantify this effect, we measured the change in capacitance between two fibers after incrementally twisting them. Figure 2b plots the change in capacitance per length (end-to-end length of the fiber) as a function of torsional level. The torsional level is the number of radians (from twisting) normalized by the end-to-end length; for example, one full twist (2π) would have a torsional level of ≈60 rad m^{-1} for a 10 cm fiber bundle. The plot includes data for pairs of intertwined fibers with three different outer diameters and their respective regression lines.

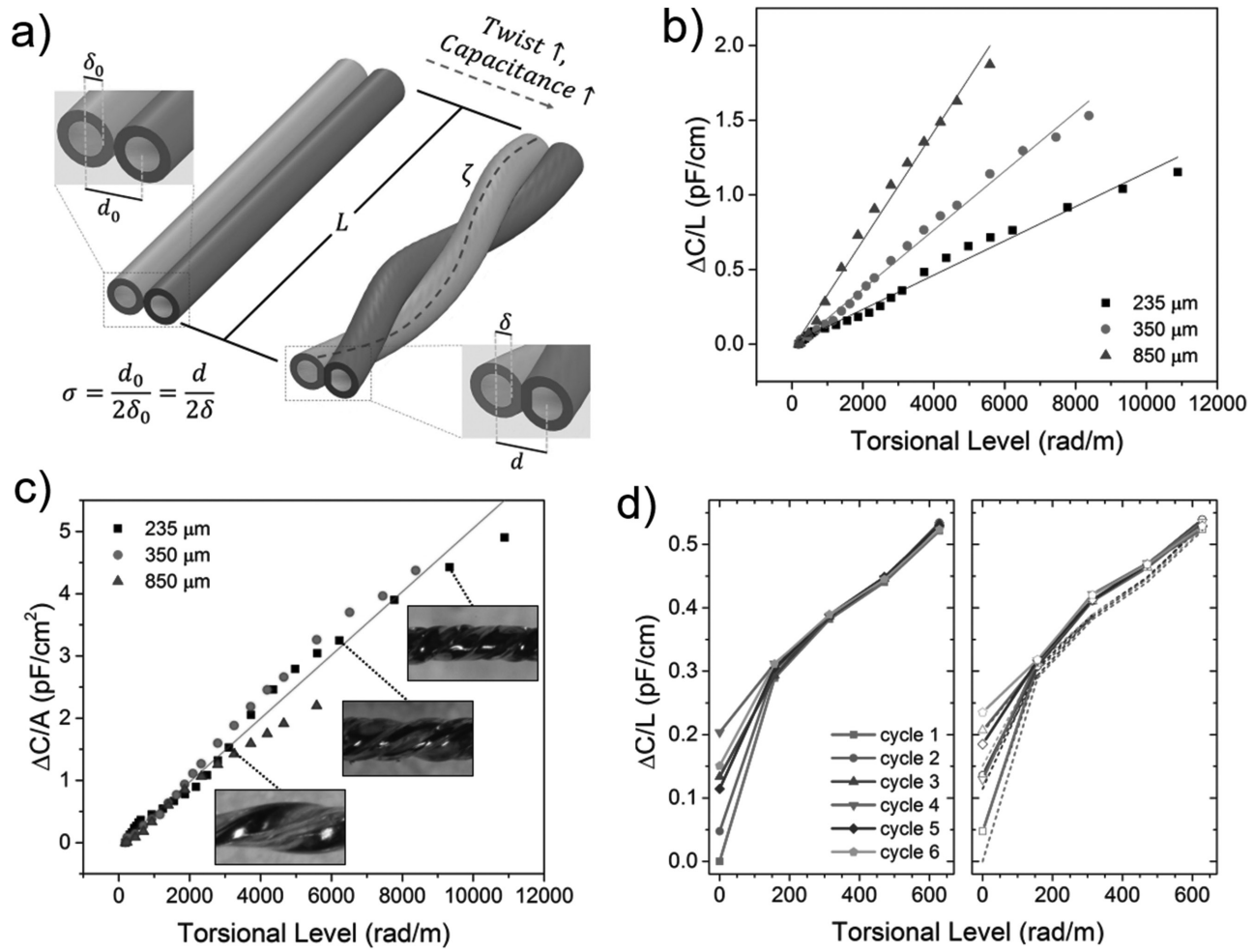

Figure 2. Two twisted fibers form a torsion sensor. a) Schematic of the torsion sensing mechanism. Changes in geometry by twisting increase the capacitance between the intertwined fibers. b) A plot of capacitance change per length (L) versus torsional level for fibers of three different diameters. Regression lines are drawn for each diameter. c) Capacitance change per length normalized by the diameter of the fibers collapses the data onto a regression line. d) A pair of fibers is repeatedly twisted and untwisted. The left graph shows the increasing torsion values for each cycle with closed markers. The right graph shows the decreasing torsion values with open markers and the increasing torsion values with dashed lines for each cycle.

The change in capacitance per length is reported relative to the value at 200 rad m^{-1}, rather than 0 rad m^{-1}, because the capacitance is highly variable at 0 rad m^{-1} since there is no tension holding the fibers together. Calculating the change in capacitance has the additional benefit of removing any stray capacitance effects from the copper wires or leads, since these effects remain constant throughout the experiment.

The change in capacitance per length varies linearly with the torsional level. The slopes of the best fit are $(1.15 \pm 0.03) \times 10^{-4}$, $(1.97 \pm 0.04) \times 10^{-4}$, and $(3.64 \pm 0.11) \times 10^{-4} \frac{\text{pF cm}^{-1}}{\text{rad m}^{-1}}$ for the 235, 350, and 850 µm diameter fibers, respectively, which show that the change in capacitance for a given change in torsional level increases as fiber diameter increases. All three regressions have an R^2 value of 0.99, although the regressions slightly overestimate the capacitance at low and high torsional levels and underestimate the capacitance at middle torsional levels, which could be related to non-Hookean mechanics. These nonlinearities, however, fall within the standard error of the measurements and are beyond the scope of this paper.

The detection limits (i.e., detecting changes to the rad m^{-1} of the twisted fibers from measurements of pF cm^{-1}) for each sensor arise by calculating the standard error for a single observation and then creating a 95% confidence interval in pF cm^{-1}. Using the slope found by the regression, we converted this interval into rad m^{-1} to find detection limits of 609, 355, and 302 rad m^{-1} for the 235, 350, and 850 µm diameter fibers, respectively. A detection limit of 302 rad m^{-1}, for example, implies the ability to sense a change in torsional level after five complete twists (for a fiber 10 cm long).

The results of Figure 2 demonstrate that the diameter of the fibers influences capacitive sensing. Fibers with larger diameters have better (lower) detection limits; however, fibers with smaller diameters can sense a larger range of torsion. This result is expected: all things being otherwise equal, fibers with larger diameters must travel a longer physical path when twisted. Since the end-to-end distances of the fiber bundles are held constant, the larger diameter fibers are subject to more stress at a given torsional level. Therefore, fibers with smaller diameters can sense a larger range of torsion before mechanical failure. In

contrast, the larger diameter fibers experience a larger change in capacitance with each additional twist, since the amount of additional stress (and thus deformation) is higher, and therefore larger diameter fibers have better (lower) detection limits.

The maximum value of torsion before mechanical failure was 10887, 8378, and 5585 rad m^{-1} for the 235, 350, and 850 μm diameter fibers, respectively. These torsional levels are one to two orders of magnitude larger than previously reported torsion sensors, which we attribute to the soft and deformable nature of the materials employed here.

To better understand the sensing mechanism, we developed a quantitative model that describes the capacitance of the fibers as a function of their torsional level. Since the fiber shape deforms during twisting, we assume that the triangular cross-section can be roughly approximated by a circle. Additionally, since the fibers are identical, the distance between the fiber centers is roughly equivalent to the diameter of a single fiber, d. Thus, to a first approximation, the capacitance between two fibers can be modeled using the equation for the capacitance, C, between two long cylindrical wires[57]

$$\frac{C}{\zeta} = \frac{\pi\varepsilon}{\ln\left(\frac{d}{2\delta} + \sqrt{\frac{d^2}{4\delta^2} - 1}\right)} \tag{1}$$

The insulated wires are in contact over length ζ (note: when twisted, the two fibers adopt the shape of a double helix and thus ζ is their helical length and is greater than the end to end distance, L, which is constant). In Equation (1), d represents the distance between the center of the two wires (in our case, the diameter of the fibers), δ represents the radius of the wire (in our case, the radius of the LM inside the fiber), and ε represents the dielectric constant of the polymer. Figure 2a depicts these geometrical parameters.

Next, we assume that the outer diameter of a fiber divided by the diameter of the EGaIn inside is a constant ratio σ (i.e., during twisting and thus, elongation of the fiber, the cross-section of the fiber shrinks uniformly)

$$\sigma = \frac{d}{2\delta} \tag{2}$$

Consequently, Equation (1) simplifies to

$$\frac{C}{\zeta} = \frac{\pi\varepsilon}{\ln\left(\sigma + \sqrt{\sigma^2 - 1}\right)} = \gamma \tag{3}$$

where γ is a constant. Thus, we can write

$$C = \gamma\zeta \tag{4}$$

Equation (4) indicates that the capacitance between the two fibers is proportional to the fiber length, which becomes longer during twisting. The length, ζ, of a single fiber in the double helix can be estimated using the equation for the arc length of a single helix, where n is the number of full turns. A derivation of Equation (5) is given in the Supporting Information

$$\zeta = \sqrt{(\pi n d)^2 + L^2} \tag{5}$$

By substituting in for torsional level given by Equation (6)

$$\tau = \frac{2\pi n}{L} \tag{6}$$

Equation (5) becomes

$$\zeta = \frac{L}{2}\sqrt{(\tau d)^2 + 4} \tag{7}$$

Combining Equations (4) and (7), results in Equation (8)

$$\frac{C}{L} = \frac{\gamma}{2}\sqrt{(\tau d)^2 + 4} \tag{8}$$

According to Equation (8), to a first-order approximation, the capacitance changes linearly with respect to τ, which is consistent with the linear response reported in Figure 2b. To determine if the model matched quantitatively, we calculated the value of γ predicted by Equation (3) for each diameter fiber, using a dielectric constant of 4.5,[58] and compared it with the experimental values of γ. The latter is found from the intercepts of the best linear fits of measured capacitance per length versus torsional level for each diameter fiber (i.e., per Equation (8) evaluated at $\tau = 0$ torsion). The predicted values of γ are 1.012, 1.179, 1.202 pF cm^{-1}, which agree well with the experimental values of 0.91 ± 0.01, 0.80 ± 0.02, and 1.02 ± 0.03 pF cm^{-1} for the 235, 350, and 850 μm fibers, respectively.

To further verify the model, we also compared the experimental slopes in Figure 2b with those predicted from Equation (8). The latter gives slopes of $(6.1 \pm 0.1) \times 10^{-5}$, $(1.20 \pm 0.02) \times 10^{-4}$, and $(3.70 \pm 0.07) \times 10^{-4}$ $\frac{\text{pF cm}^{-1}}{\text{rad m}^{-1}}$ for the 235, 350, and 850 μm diameter fibers, respectively. The experimental slopes in Figure 2b agree well with these predicted values. As the fiber diameter increases, there is improved agreement between the experimental slope and predicted slope (in the case of the 850 μm fiber, the values are practically identical), which likely results from the cross-section of larger diameter fibers better resembling the circular cross-section used in the model. Additionally, Equation (8) predicts that the model will become more linear when the term $(\tau d)^2$ is much greater than 4 (the other term under the square root); this condition is satisfied with larger diameters (d).

Equation (8) does not capture several potential sources of error, including the removal of void space that occurs at low torsional levels and the creation of capacitance between the wires both perpendicular and parallel to the fiber axis at high torsional levels. Nevertheless, the general linear increase in capacitance with torsion, the measured values of γ, and the measured slopes for each diameter fiber are consistent with the predictions given by Equation (8).

Equation (8) also suggests that the slope of the data plotted in Figure 2b should be roughly proportional to fiber diameter. We therefore normalized the data by dividing the change in capacitance per length (end-to-end) by the original fiber

diameter to give change in capacitance per initial contact area. Figure 2c plots the change in capacitance per area as a function of torsional level for all three diameter fibers. The data points collapse into a single regression with a slope of $(5.10 \pm 0.11) \times 10^{-4}$ pF cm^{-2} and an R^2 value of 0.99. Images of the 235 µm fibers at 3110, 6221, and 9332 rad m^{-1} are shown as insets in Figure 2c (1 mm of length shown).

We also explored the repeatability of the sensors after multiple cycles of twisting and untwisting. Figure 2d plots the change in capacitance per length for a pair of 850 µm diameter intertwined fibers that were twisted and untwisted for six consecutive cycles. Overall, the sensing is reproducible despite being twisted by hand. At low torsional levels, a large amount of variation occurs between cycles due to the gaps that appear between the fibers after each cycle at zero torsion. This separation arbitrarily changes the contact area and thereby the capacitance. Additionally, since the fiber cross-sections are not perfect circles, the changes in the orientation of the fiber that occur at low torsional levels can create corner-edge contact between the fibers as opposed to the preferred face-to-face contact (which minimizes the center to center distance of the fibers and maximizes the contact area) that occurs at higher torsional levels. At torsional levels beyond 200 rad m^{-1}, we observe more consistent behavior between cycles, which indicates a decrease in void spaces and corner-edge contacts. The small discrepancy between the increasing and decreasing torsion may be attributed to a time-dependent hysteresis that occurs as the fibers are untwisted (i.e., it takes a certain amount of time for the untwisted fibers to return to their original state via decompression due to the friction between fibers). We also investigated the sensitivity of the sensor to temperature between −10 and 25 °C, and found that capacitive output decreased roughly 0.0003 pF cm^{-1} for each 1 °C decrease in temperature. This is 0.27% per °C of the detection limit of the sensor, which implies that the sensor performance should be relatively independent of temperature over this range.

2.2. Strain Sensor

In addition to measuring torsion, two intertwined fibers may also be used to measure strain due to the increase in contact area from elongation. To measure the change in capacitance with respect to strain, we intertwined two fibers to a set initial torsional level and then increased the end-to-end length in intervals of 20% while measuring the capacitance. Elongating the fibers increases the contact area between them, resulting in increased capacitance.

Figure 3a plots the capacitance per initial length as a function of percentage strain for a pair of 850 µm diameter fibers at different torsional levels and their respective regression lines. At an initial torsional level of 0 rad m^{-1}, there is not a statistically significant relationship between strain and capacitance due to the presence of void space between fibers; however, at higher initial torsional levels, the fibers are in intimate contact and a linear relationship emerges. The slopes are $(7.1 \pm 0.2) \times 10^{-3}$, $(8.7 \pm 0.4) \times 10^{-3}$, $(9.5 \pm 0.2) \times 10^{-3}$, $(9.8 \pm 0.2) \times 10^{-3}$, and $(1.01 \pm 0.01) \times 10^{-2}$ pF cm^{-1} for the initial torsional levels of 314, 628, 942, 1257, and 1571 rad m^{-1}, respectively. All of the regressions had an R^2 value of 0.99. The detection limits were 5.89%, 9.45%, 5.17%, 4.06%, and 2.90% of strain, respectively. A gauge factor—the change in signal normalized by strain—was calculated by dividing the change in capacitance by the base capacitance and dividing again by the strain, and was found to be between 0.66 and 0.82 for all initial torsional levels except 0 rad m^{-1}.

This linear change can be predicted by adapting Equation (4) to account for the change in capacitance from C_0 to C_f due to the change in length from ζ_0 to ζ_f

$$\Delta C = C_f - C_0 = \gamma(\zeta_f - \zeta_0) \tag{9}$$

Using Equations (5) and (9) while noting that the end-to-end length of the fibers is no longer constant, we can derive the following equation (full derivation in the Supporting Information)

$$\frac{\Delta C}{L_0} = \frac{\gamma}{2}\left[\sqrt{(\tau_0 d)^2 + \frac{4L_f^2}{L_0^2}} - \sqrt{(\tau_0 d_0)^2 + 4}\right] \tag{10}$$

Assuming a Poisson ratio of 0.5 to conserve volume, we can substitute for d with the expression given by Equation (11) (full derivation given in the Supporting Information)

$$d = d_0\left(\frac{L_0}{L_f}\right)^{0.5} \tag{11}$$

Thus, Equation (10) simplifies to

$$\frac{\Delta C}{L_0} = \frac{\gamma}{2}\left[\sqrt{(\tau_0 d_0)^2 \frac{L_0}{L_f} + \frac{4L_f^2}{L_0^2}} - \sqrt{(\tau_0 d_0)^2 + 4}\right] \tag{12}$$

The parameters in Equation (12) are all constant except for L_f and ΔC, which change with elongation. Furthermore, the first term on the right-hand side of Equation (12) (under the first square root) is significantly smaller than the second term at the torsional levels used here. It decreases in size as strain increases and thus becomes even less relevant. Thus, to a first-order approximation, Equation (12) predicts that the change in capacitance will change linearly with respect to elongation (L_f). Figure 3b–d compares the predicted values from Equation (12) to the experimental change in capacitance per length as a function of percentage strain for three different torsional levels. As the torsional level increases, the agreement between the theoretical Equation (12) and the experimental data improves, likely due to the removal of void space and corner-edge contacts between the fibers, for which the theoretical model does not account.

2.3. Touch Sensor

There are also other ways to use fibers for capacitive sensing. As an example, we fabricated a touch sensor from

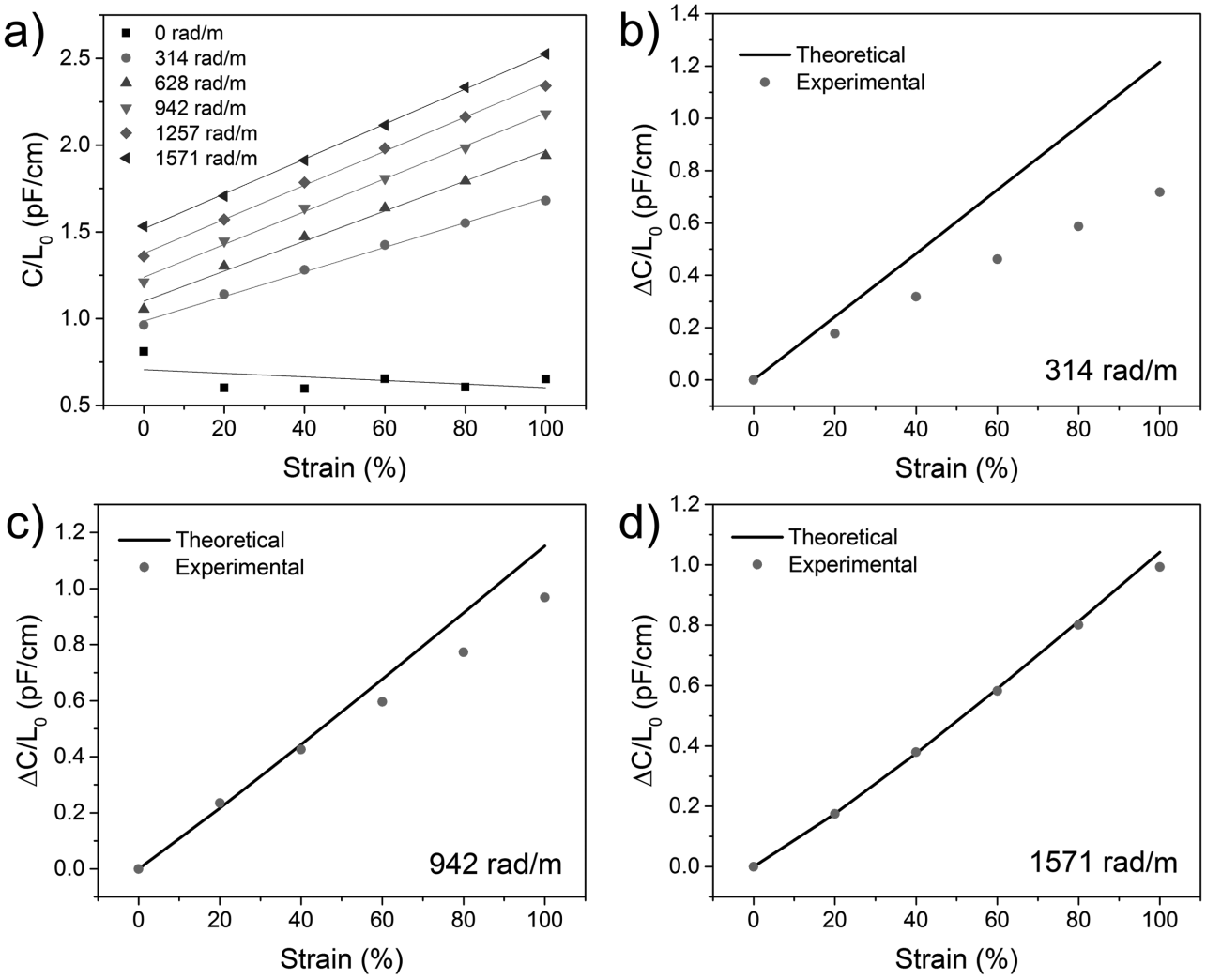

Figure 3. Two twisted fibers (850 µm diameter) form a capacitive strain sensor due to the increase in contact area from elongation. a) A plot of capacitance per initial length versus strain for fibers at various torsional levels with regression lines plotted for each level. b–d) Theoretical and experimental comparison of change in capacitance per initial length as a function of strain for three different initial torsional levels, 314, 942, and 1571 rad m^{-1}, respectively.

three intertwined fibers in a triple helix. **Figure 4**a depicts three fibers (A, B, C) filled to different lengths with EGaIn. Fiber A is filled one-third of the way, Fiber B is filled two-thirds of the way, and Fiber C is fully filled. In Region III, all three fibers are filled, while in Regions II and I only two fibers (B and C) and one fiber (C) are filled, respectively. The presence of EGaIn in the fiber allows for a capacitor to be formed between the fiber and a lightly touching finger (i.e., self-capacitance), without the need for physical deformation. Thus, when a finger touches Region III, all three fibers will report an increase in capacitance since all three contain LM in that region, whereas when a finger touches Region I, only the fiber containing LM (C) will report an increase in capacitance. Figure 4b shows a finger touching each region, which is detected by the sensor and results in the illumination of the corresponding light-emitting diode (LED) light. The LEDs and the fibers are connected to an Arduino microcontroller, which reads the change in capacitance from each fiber and sends an output signal to illuminate the correct LED when the appropriate region of the fiber is touched (more details given in the Supporting Information). Video S1 (Supporting Information) shows a demonstration of this stretchable touch sensor.

Figure 4c shows a graph of capacitance as a function of time for a one-third filled, two-thirds filled, and fully filled fiber marked as A, B, and C, respectively. Examination of the graph allows one to clearly identify Region III (where all three fibers show an increase in capacitance), Region II (where only two fibers show an increase in capacitance), and Region I (where only one fiber shows an increase in capacitance). The change in capacitance is ≈0.8 pF, slightly less than the 2 pF change measured in conventional touch screens. There is additional variance in the A and B lines compared to the C line, most likely due to the stray capacitance and edge effects that occur since these fibers are not filled completely. This variance, however, does not prevent the sensor from distinguishing between the

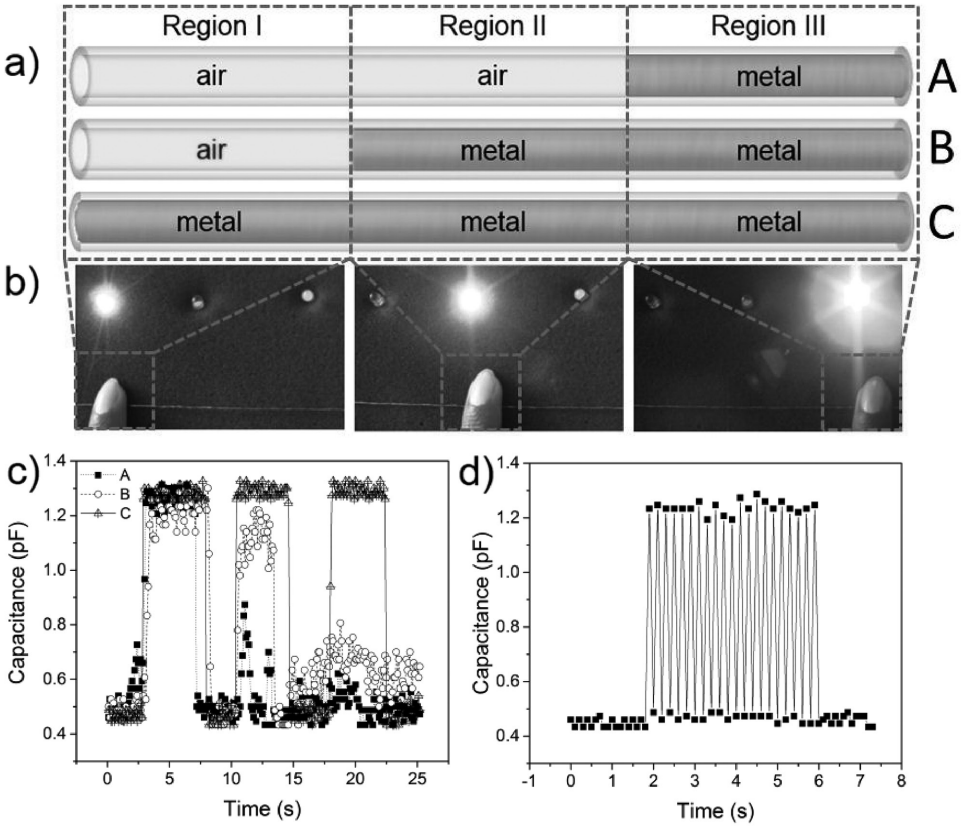

Figure 4. Three twisted fibers (235 µm diameter) create a sensor able to differentiate regions of touch along its length by self-capacitance. a) Three distinct regions (I, II, III) along three intertwined fibers are created by varying the distance of EGaIn in each fiber. Fibers A, B, and C are one-third filled, two-thirds filled, and fully filled with EGaIn, respectively. b) As each region is touched, the sensor responds by illuminating the correct LED. c) A plot of capacitance versus time shows the change in capacitance as each region of the fiber bundle (III, II, and I) is touched for a one-third filled, two-thirds filled, and fully filled fiber. d) A plot of capacitance versus time for a single fiber undergoing rapid tapping shows capacitance jumps in 100 ms intervals.

different regions. Figure 4d plots capacitance versus time for a single fiber as it undergoes rapid tapping in 100 ms intervals, showing that the fiber can respond rapidly to touch.

3. Conclusion

This paper describes the fabrication and characterization of soft and stretchable capacitive sensors of torsion, strain, and touch using hollow elastomeric fibers filled with LM. Twisting or elongating an intertwined bundle of two fibers increases the contact area between the fibers and therefore the capacitance. Additionally, bundles of fibers filled with LM can serve as capacitive touch sensors along the length of the bundle by using fibers filled with metal to various lengths. These sensors detect touch via self-capacitance with the finger, rather than by physical deformation. Because these fiber sensors are extremely soft and stretchable, as well as small (≈200–800 µm diameter), they could be used with artificial muscles, soft robotics, and stretchable devices. They have higher detection limits than state-of-the-art sensors; however, they can measure large ranges of torsion and strain and have an advantageous fiber shape that can conform to a variety of complex surfaces. As the modes for sensing torsion, strain, and touch all rely on capacitance, it is currently not possible to decouple them, though future work could measure other electrical properties, such as resistance, to help decouple their effects. For these fibers to be utilized in fabrics, further work must be done to understand their cyclic behavior and wash resistance; however, these fibers offer a promising opportunity to create woven and wearable sensors in stretchable textiles for a variety of sensing functions.

Supporting Information

Supporting Information is available from the Wiley Online Library or from the author.

Acknowledgements

The authors acknowledge support from the Army Natick (W911QY-14-C-0033) for this work. The authors also acknowledge Russell Mailen for assistance with the creation of Figure 2a.

Received: October 27, 2016
Revised: February 9, 2017
Published online: March 23, 2017

[1] D.-H. Kim, N. Lu, R. Ma, Y.-S. Kim, R.-H. Kim, S. Wang, J. Wu, S. M. Won, H. Tao, A. Islam, K. J. Yu, T. Kim, R. Chowdhury, M. Ying, L. Xu, M. Li, H.-J. Chung, H. Keum, M. McCormick, P. Liu, Y.-W. Zhang, F. G. Omenetto, Y. Huang, T. Coleman, J. A. Rogers, *Science* **2011**, *333*, 838.
[2] Y. Cheng, R. Wang, J. Sun, L. Gao, *Adv. Mater.* **2015**, *27*, 7365.
[3] C. S. Boland, U. Khan, C. Backes, A. O'Neill, J. McCauley, S. Duane, R. Shanker, Y. Liu, I. Jurewicz, A. B. Dalton, J. N. Coleman, *ACS Nano* **2014**, *8*, 8819.
[4] M. Amjadi, A. Pichitpajongkit, S. Lee, S. Ryu, I. Park, *ACS Nano* **2014**, *8*, 5154.
[5] W. Gao, S. Emaminejad, H. Y. Y. Nyein, S. Challa, K. Chen, A. Peck, H. M. Fahad, H. Ota, H. Shiraki, D. Kiriya, D.-H. Lien, G. A. Brooks, R. W. Davis, A. Javey, *Nature* **2016**, *529*, 509.
[6] R. C. Webb, A. P. Bonifas, A. Behnaz, Y. Zhang, K. J. Yu, H. Cheng, M. Shi, Z. Bian, Z. Liu, Y.-S. Kim, W.-H. Yeo, J. S. Park, J. Song, Y. Li, Y. Huang, A. M. Gorbach, J. A. Rogers, *Nat. Mater.* **2013**, *12*, 938.
[7] Z. F. Liu, S. Fang, F. A. Moura, J. N. Ding, N. Jiang, J. Di, M. Zhang, X. Lepró, D. S. Galvão, C. S. Haines, N. Y. Yuan, S. G. Yin, D. W. Lee, R. Wang, H. Y. Wang, W. Lv, C. Dong, R. C. Zhang, M. J. Chen, Q. Yin, Y. T. Chong, R. Zhang, X. Wang, M. D. Lima, R. Ovalle-Robles, D. Qian, H. Lu, R. H. Baughman, *Science* **2015**, *349*, 400.
[8] T. Yamada, Y. Hayamizu, Y. Yamamoto, Y. Yomogida, A. Izadi-Najafabadi, D. N. Futaba, K. Hata, *Nat. Nanotechnol.* **2011**, *6*, 296.
[9] S. Gong, W. Schwalb, Y. Wang, Y. Chen, Y. Tang, J. Si, B. Shirinzadeh, W. Cheng, *Nat. Commun.* **2014**, *5*, 3132.
[10] M. D. Dickey, *ACS Appl. Mater. Interfaces* **2014**, *6*, 18369.
[11] Y. Lu, Q. Hu, Y. Lin, D. B. Pacardo, C. Wang, W. Sun, F. S. Ligler, M. D. Dickey, Z. Gu, *Nat. Commun.* **2015**, *6*, 10066.
[12] W. Zeng, L. Shu, Q. Li, S. Chen, F. Wang, X.-M. Tao, *Adv. Mater.* **2014**, *26*, 5310.
[13] L. M. Castano, A. B. Flatau, *Smart Mater. Struct.* **2014**, *23*, 53001.
[14] Y. Wei, S. Chen, X. Yuan, P. Wang, L. Liu, *Adv. Funct. Mater.* **2016**, *26*, 5078.
[15] Y. Tai, G. Lubineau, *Adv. Funct. Mater.* **2016**, *26*, 4078.
[16] Y. Lin, C. Ladd, S. Wang, A. Martin, J. Genzer, S. A. Khan, M. D. Dickey, *Extreme Mech. Lett.* **2016**, *7*, 55.
[17] M. Park, J. Im, M. Shin, Y. Min, J. Park, H. Cho, S. Park, M.-B. Shim, S. Jeon, D.-Y. Chung, J. Bae, J. Park, U. Jeong, K. Kim, *Nat. Nanotechnol.* **2012**, *7*, 803.
[18] S. Zhu, J.-H. So, R. Mays, S. Desai, W. R. Barnes, B. Pourdeyhimi, M. D. Dickey, *Adv. Funct. Mater.* **2013**, *23*, 2308.
[19] T. Yang, Y. Wang, X. Li, Y. Zhang, X. Li, K. Wang, D. Wu, H. Jin, Z. Li, H. Zhu, *Nanoscale* **2014**, *6*, 13053.
[20] T. Yamada, Y. Yamamoto, Y. Hayamizu, A. Sekiguchi, H. Tanaka, K. Kobashi, D. N. Futaba, K. Hata, *ACS Nano* **2013**, *7*, 3177.
[21] L. A. Wang, C. Y. Lin, G. W. Chern, *Meas. Sci. Technol.* **2001**, *12*, 793.
[22] H. Scherr, G. Scholl, F. Seifert, R. Weigel, in *IEEE Ultrason. Symp., Proc.*, IEEE, New York **1996**, *1*, 347.
[23] H. Wakiwaka, M. Mitamura, *Sens. Actuators, A* **2001**, *91*, 103.
[24] D. Rus, M. T. Tolley, *Nature* **2015**, *521*, 467.
[25] R. K. Kramer, SPIE Proceedings, *Soft electronic for soft robotics*, Vol. *9467*, in (Eds: T. George, A. K. Dutta, M. S. Islam), SPIE, Bellingham, WA, **2015**, p. 946707.
[26] C. S. Haines, M. D. Lima, N. Li, G. M. Spinks, J. Foroughi, J. D. W. Madden, S. H. Kim, S. Fang, M. J. de Andrade, F. Göktepe, Ö. Göktepe, S. M. Mirvakili, S. Naficy, X. Lepró, J. Oh, M. E. Kozlov, S. J. Kim, X. Xu, B. J. Swedlove, G. G. Wallace, R. H. Baughman, *Science* **2014**, *343*, 868.
[27] J. Park, I. You, S. Shin, U. Jeong, *ChemPhysChem* **2015**, *16*, 1155.
[28] B. Lee, *Opt. Fiber Technol.* **2003**, *9*, 57.
[29] J.-H. So, J. Thelen, A. Qusba, G. J. Hayes, G. Lazzi, M. D. Dickey, *Adv. Funct. Mater.* **2009**, *19*, 3632.
[30] M. G. Mohammed, M. D. Dickey, *Sens. Actuators, A* **2013**, *193*, 246.
[31] H. Ota, K. Chen, Y. Lin, D. Kiriya, H. Shiraki, Z. Yu, T.-J. Ha, A. Javey, *Nat. Commun.* **2014**, *5*, 5032.
[32] J. T. B. Overvelde, Y. Mengüç, P. Polygerinos, Y. Wang, Z. Wang, C. J. Walsh, R. J. Wood, K. Bertoldi, *Extreme Mech. Lett.* **2014**, *1*, 42.
[33] C. To, T. L. Hellebrekers, Y. L. Park, in *2015 IEEERSJ Int. Conf. Intelligent Robots Systems IROS*, **2015**, pp. 5898–5903.
[34] X. Xiao, L. Yuan, J. Zhong, T. Ding, Y. Liu, Z. Cai, Y. Rong, H. Han, J. Zhou, Z. L. Wang, *Adv. Mater.* **2011**, *23*, 5440.
[35] Y. R. Jeong, H. Park, S. W. Jin, S. Y. Hong, S.-S. Lee, J. S. Ha, *Adv. Funct. Mater.* **2015**, *25*, 4228.
[36] Y. Menguc, Y.-L. Park, H. Pei, D. Vogt, P. M. Aubin, E. Winchell, L. Fluke, L. Stirling, R. J. Wood, C. J. Walsh, *Int. J. Rob. Res.* **2014**, *33*, 1748.
[37] Y.-L. Park, B.-R. Chen, R. J. Wood, *IEEE Sens. J.* **2012**, *12*, 2711.
[38] J.-B. Chossat, Y.-L. Park, R. J. Wood, V. Duchaine, *IEEE Sens. J.* **2013**, *13*, 3405.
[39] R. K. Kramer, C. Majidi, R. Sahai, R. J. Wood, in *2011 IEEERSJ Int. Conf. Intelligent Robots Systems IROS*, IEEE, New York, **2011**, pp. 1919–1926.
[40] C. Majidi, R. Kramer, R. J. Wood, *Smart Mater. Struct.* **2011**, *20*, 105017.
[41] Y. Jiao, C. Young, S. Yang, S. Oren, H. Ceylan, S. Kim, K. Gopalakrishnan, P. Taylor, L. Dong, *IEEE Sens. J.* **2016**, *16*, 7870.
[42] D. J. Lipomi, M. Vosgueritchian, B. C.-K. Tee, S. L. Hellstrom, J. A. Lee, C. H. Fox, Z. Bao, *Nat. Nanotechnol.* **2011**, *6*, 788.
[43] D. J. Cohen, D. Mitra, K. Peterson, M. M. Maharbiz, *Nano Lett.* **2012**, *12*, 1821.
[44] L. Cai, L. Song, P. Luan, Q. Zhang, N. Zhang, Q. Gao, D. Zhao, X. Zhang, M. Tu, F. Yang, W. Zhou, Q. Fan, J. Luo, W. Zhou, P. M. Ajayan, S. Xie, *Sci. Rep.* **2013**, *3*, 3048.
[45] S. Yao, Y. Zhu, *Nanoscale* **2014**, *6*, 2345.
[46] A. Frutiger, J. T. Muth, D. M. Vogt, Y. Mengüç, A. Campo, A. D. Valentine, C. J. Walsh, J. A. Lewis, *Adv. Mater.* **2015**, *27*, 2440.
[47] K. K. Kim, S. Hong, H. M. Cho, J. Lee, Y. D. Suh, J. Ham, S. H. Ko, *Nano Lett.* **2015**, *15*, 5240.
[48] A. Fassler, C. Majidi, *Smart Mater. Struct.* **2013**, *22*, 55023.
[49] S. Liu, X. Sun, O. J. Hildreth, K. Rykaczewski, *Lab Chip* **2015**, *15*, 1376.
[50] S. Takamatsu, T. Kobayashi, N. Shibayama, K. Miyake, T. Itoh, in *2011 Symp. Design, Test, Integration Packaging MEMS/MOEMS (DTIP)*, IEEE, New York, **2011**, pp. 142–147.
[51] X. Wang, T. Li, J. Adams, J. Yang, *J. Mater. Chem. A* **2013**, *1*, 3580.
[52] L. Viry, A. Levi, M. Totaro, A. Mondini, V. Mattoli, B. Mazzolai, L. Beccai, *Adv. Mater.* **2014**, *26*, 2659.
[53] S. Takamatsu, T. Yamashita, T. Imai, T. Itoh, *Sens. Mater.* **2013**, *25*, 627.
[54] B. Li, Y. Gao, A. Fontecchio, Y. Visell, *Smart Mater. Struct.* **2016**, *25*, 75009.
[55] B. Li, A. K. Fontecchio, Y. Visell, *Appl. Phys. Lett.* **2016**, *108*, 13502.
[56] Y.-L. Park, D. Tepayotl-Ramirez, R. J. Wood, C. Majidi, *Appl. Phys. Lett.* **2012**, *101*, 191904.
[57] J. D. Jackson, *Classical Electrodynamics*, Wiley, New York **1962**.
[58] J. G. Drobny, *Handbook of Thermoplastic Elastomers*, William Andrew, Norwich, NY, **2007**.